Tellus (1997), 49A, 246–262

TELLUS
ISSN 0280–6495

Evaluation of model clouds and radiation at 100 km scale using GOES data

By WEI YU*, LOUIS GARAND AND ASHU P. DASTOOR, *Atmospheric Environment Service, Dorval, Quebec, Canada*

(Manuscript received 18 December 1995; in final form 10 July 1996)

ABSTRACT

Model simulated cloud properties such as cloud fraction, cloud top height, and infrared (IR) radiance are compared to those from GOES-7 satellite observations over a monthly period from an ensemble of thirty-one forecasts launched each day of October 1993. The aim is to evaluate both the above mentioned parameters and the cloud optical properties (emissivity, optical depth) in a global model that carries cloud water (ice and water phases combined) as a prognostic variable. The results show that the model simulates well the cloud fraction, cloud top height, and IR radiance in the middle and high latitude regions, especially in the Northern Hemisphere. Most obvious deficiencies are found in the tropics and subtropics over the ocean: underestimation of cloud fraction and cloud top height in the inter-tropical convergence zone, and overestimation of low clouds in the subtropics. The causes of these deficiencies are discussed. The cloud emissivity parameterization is tested and its sensitivity to effective cloud fraction and outgoing radiance is assessed from comparisons with cases that assume an emissivity of unity. The resulting global infrared budget is realistic with a net loss at the top of the atmosphere of 243 W/m^2 and 55 W/m^2 at the surface. Although error compensation between cloud height and fraction occurs in some areas to yield good IR radiances, the outgoing radiation is excellent in regions where clouds are best, thus validating the chosen emissivity parameterization. After some adjustment of the parameterized visible cloud optical depth, the global shortwave budget is also reasonable compared to available climatology with a net surface flux of 157 W/m^2 and a planetary albedo of 30%. The sensitivity to various parameters affecting the radiation budget is examined.

1. Introduction

In an effort to implement a prognostic cloud water scheme in the Canadian global operational model, an evaluation of simulated cloud properties and their radiative impact is carried out using satellite observations. A variety of satellite data can be used for that purpose such as those of the Earth Radiation Budget Experiment (ERBE) or the International Satellite Cloud Climatology Project (ISCCP) (Morcrette, 1991; Yu et al., 1991; Bony et al., 1992). For convenience, GOES-7 (Geostationary Operational Environment Satellite) data are used in the present study because they are available routinely at the Canadian Meteorological Center (CMC), and because a cloud analysis system extracts relevant measures every 6 h from these data at a 100 km resolution (Garand, 1993). This dataset is complete for the monthly period studied of October 1993. This choice of data allows one to compare systematically the model simulations with the satellite observations, and the same evaluation procedure could eventually be run as frequently as the need arises from archived satellite parameters and

* Corresponding author's address: Wei Yu, CEntre de Recherche en Calcul Appliqué (CERCA), 5160, Boul. Décarie, bureau 400, Montreal, Canada, H3X 2H9.

model forecasts. While the evaluation domain is not global, it does cover about 20% of the globe (60°N to 60°S; 50°W to 170°W). The model strengths and weaknesses for simulating cloud properties and their radiative impact are diagnosed.

A prognostic cloud water scheme based on Sundqvist et al. (1989) is used in the simulations. Both climate and weather forecast models will benefit from a model that carries cloud water as a prognostic variable; it represents a significant step towards more realism in the parameterization of cloud radiative properties. Indeed, the IR emissivity of the cloud and its visible optical depth are linked to the cloud water path (CWP). In conjunction with clouds, these two parameters control the longwave and shortwave radiation budget. Cloud fraction and cloud water are outputs of the condensation scheme as well as the layer precipitation flux. This is clearly an improvement over current diagnosed cloud fraction (from relative humidity), diagnosed cloud water (from temperature alone) and precipitation available at the surface only.

In this paper, we limit our evaluation based on satellite-model collocations to clouds and infrared radiation. A similar evaluation using the visible channel of GOES satellite needs both well calibrated data (in that respect the new GOES-8 and 9 visible sensors are superior to GOES-7) and a treatment of bi-directional reflectivity. To do this would be beyond the scope of the paper, however we did compare the model generated solar radiation budget with that of climatology obtained from satellite observations in order to ensure that the solar radiation budget would be reasonable following the major change proposed, that is, using a new cloud condensation scheme together with revised shortwave cloud optical properties. Water cycle variables (integrated water vapor, cloud water, and precipitation) were evaluated by Deblonde et al (1996) for the same month of October 1993 using microwave imagery.

The paper is organized as follows. In Section 2, a brief description of the Canadian global spectral model is presented. The following section describes the satellite data analysis system and the evaluation methodology. In Section 4, the model simulated cloud properties and infrared radiance are compared with satellite data. In Section 5, the sensitivity of the energy budget to cloud emissivity and optical depth parameterizations is assessed. The last section concludes on ways to further improve cloud parameterizations and their evaluation.

2. Model description

The Canadian global spectral model (Ritchie, 1991) is used in this study. A prognostic cloud scheme (Sundqvist et al., 1989) was implemented in this model (Dastoor, 1994); vectorization work was done to speed up the execution time to meet operation criteria. This cloud scheme calculates both deep convection and stratiform cloud condensation. A detailed description of the condensation and precipitation microphysics parameterizations can be found in Sundqvist et al. (1989). Briefly, a set of 3 equations governing the rate of change of temperature, specific humidity and cloud water is solved. The condensation algorithm branches to either the stratiform or convective part of the code according to stability criteria; the cloud and precipitation outputs are therefore either stratiform or convective in nature, i.e. no layer represents a mixture of the two regimes. In a given atmospheric column however, the output of individual layers may come from either branch.

The model predicted cloud fraction and cloud water content (outputs of the cloud condensation scheme) serve as input to the shortwave and longwave radiation codes. The infrared scheme is based on Garand (1983, see also Garand and Mailhot, 1990), with a new parameterization of cloud emissivity. In the infrared code, the transmissivity through model layers with clouds (t_c) is computed following the usual hypothesis of maximum overlapping of adjacent cloud layers and random overlapping of cloud layers separated by clear ones as originally proposed by Geleyn and Hollingsworth (1979): for two layers with cloud transmissivities t_{c1} and t_{c2} , $t_c = t_{c1}\ t_{c2}$ in the random overlapping assumption, but $t_c = \min(t_{c1}, t_{c2})$ in the maximum overlapping assumption. The impact of overlapping assumptions on the radiation fields was studied by Yu et al. (1996) and other authors; the maximum-random overlapping assumption is judged to be the most realistic especially with a high number of layers. An individual layer (l) with cloud fraction (CF_l) has a transmissivity:

$$t_{c1} = (1 - CF_1 \varepsilon_1), \quad (1)$$

where ε_l is cloud emissivity. The emissivity of water clouds (ε_w) is parameterized following Stephens (1978):

$$\varepsilon_w = 1 - \exp(-0.0783 \sec(\beta) \mathrm{LWP}), \tag{2}$$

where β is the satellite viewing angle (in the calculation of flux as opposed to radiance $\sec(\beta)$ is replaced with the diffusivity factor 1.66). LWP is the liquid water path computed at nadir expressed in g/m^2 and is obtained directly from the cloud water content, CWC (kg of water per kg of air) as follows:

$$LWP = f_w CWC \frac{dp}{g}, \tag{3}$$

where g is the gravitational acceleration, dp is the pressure thickness and f_w the liquid water fraction of CWC. f_w is taken to be a function of the temperature of the layer as suggested by Rockel et al. (1991):

$$f_w = 0.0059 + 09941 \exp(-0.003102\ T_i^2), \tag{4}$$

with T_i in Celsius. The ice emissivity ε_i for the 11 μm band is parameterized following Ebert and Curry (1992):

$$\varepsilon_i = 1 - \exp(-\sec(\beta) k \mathrm{IWP}), \tag{5}$$

with $k = 0.0003 + 1.29/r_e$. IWP is the ice water path computed as LWP except that f_w is replaced with $(1 - f_w)$ in eq. (3). An effective radius r_e of 25 μm is assumed for ice particles. Since the total cloud transmissivity is the product of the ice and water components, the combined ice-water emissivity (ε_l) is obtained from:

$$\varepsilon_l = 1 - (1 - \varepsilon_i)(1 - \varepsilon_w) \tag{6}$$

Obviously, there are uncertainties related to these formulas, especially with regards to the ice emissivity. An additional goal of this study is to examine the sensitivity of these parameterizations to the IR budget.

The solar radiation scheme is based on Fouquart and Bonnel (1980) supplemented by a parameterization of cloud optical properties which are functions of cloud water content. Clouds are assumed to be plane-parallel, and random overlapping of cloud layers is assumed. A subgrid distribution of cloud water is considered, that is to say the cloud water content addressed in both solar and infrared radiation computation is always the in-cloud value (output of cloud condensation scheme devised by cloud fraction, see Sundqvist et al. (1989) for the concept of subgrid value). There are three basic shortwave cloud optical parameters used in radiation codes: the asymmetry factor, G (capitalized here to distinguish from the gravitational constant), the single scattering albedo (ω) and the optical depth (δ). Many parameterizations are proposed for these parameters in the literature, most of them related to the water or ice water path and to the effective droplet radius r_e defined as the ratio of the third to second moment of the cloud drop size distribution. These parameterizations are wavelength dependent. As our radiation code parameterizes the entire solar domain in one spectral interval, needed optical properties are broad band equivalent ones.

For pure water clouds, we use the formalism proposed by Slingo (1989) to characterize the cloud shortwave radiative properties.

$$\delta = \mathrm{LWP}\left(a + \frac{b}{r_{e_w}}\right), \tag{7}$$

$$1 - \omega = c + \mathrm{d} r_{e_w}, \tag{8}$$

$$G = e + f r_{e_w}, \tag{9}$$

where a-f are broad band constants listed in Table 1 obtained by averaging the individual spectral band values using weights proportional to the fraction of solar energy in each band (spectral values and weights taken from Slingo, 1989). LWP is the liquid water path expressed in g/m^2. The effective radius of water clouds (r_{e_w}) is parameterized assuming a Gamma distribution (see Barker, 1992) verified to be realistic from aircraft measurements of water droplet spectra:

$$r_{e_w} = 754.6 \left(\frac{\mathrm{LWC} d_a}{N}\right)^{1/3} \tag{10}$$

with r_{e_w} in μm, d_a the air density in kg/m^3 and N the number of cloud drops per cm^3 taken as 100 over oceans and 500 over land. LWC is the liquid water content expressed in kg/kg. Values in the range 4–17 μm are acceptable for r_{e_w}; this is the range of validity of Slingo (1989) parameterizations.

For pure ice clouds, we follow Ebert and Curry (1992), using identical equations (7–9) to those derived for the parameterization for water clouds; their study assumed hexagonal ice crystals. The values of constants a-f are listed in Table 1; averaging to get values representative of the entire

Table 1. *Values of coefficients in eqs. (7–9) for water and ice clouds*

	a (m^2g^{-1})	b ($\mu m\ m^2g^{-1}$)	c	d (μm^{-1})	e	f (μm^{-1})
pure water	2.622×10^{-2}	1.356	6.814×10^{-3}	4.842×10^{-4}	0.804	3.850×10^{-3}
pure ice	3.448×10^{-3}	2.431	1.295×10^{-2}	1.321×10^{-4}	0.777	5.897×10^{-4}

solar spectrum was done in the same manner as for water clouds. In the absence of established parameterizations for the effective radius of ice clouds, r_{e_i} is set to 25 μm, the value already quoted for the infrared ice emissivity parameterization.

For mixed clouds, as in Rockel et al (1991), the radiative properties (eqs. (7–9)) are calculated respectively for the fraction of the available total CWC (eq. (4)) attributed to water and ice clouds. The ice and water optical depths are then summed, the single scattering albedos for each phase are weighted by their corresponding optical depths and the asymmetry factors by their corresponding product $\delta\omega$. The three parameters are then passed to the solar radiation code. Of the three parameters, the optical depth is certainly the most important in terms of impact on the net fluxes at the surface and at the top of the atmosphere. Second in importance is the single scattering albedo which influences directly the atmospheric heating and planetary albedo, but the surface flux to a lower degree. In comparison to the other two parameters, the asymmetry factor has a relatively modest impact.

3. Cloud analysis and model evaluation system

3.1. *GOES cloud parameters*

At the CMC, an operational system extracts cloud and radiation parameters every six hours from the visible, infrared window (11 μm) and water vapor (6.7 μm) bands of GOES-7 which was positioned at 110°W in October 1993. The system, named Humsat, was originally built to obtain humidity profiles in a statistical manner based on cloud classification (Garand, 1993; Deblonde et al, 1995). These humidity profiles are assimilated operationally and therefore influence the analyses for the October 1993 month under study. The parameters of interest for this study are the total cloud fraction (CF), the cloud top height (HT), and the equivalent 11 μm brightness temperature (TB) derived from the radiance of GOES-7 averaged over an area of 1 × 1 degree. CF, HT, and TB are not directly used in the analysis, only derived humidity profiles. Only the data at 00 UTC are used in the evaluation because we want to evaluate twenty-four hour forecasts and because visible imagery is available at that time over most of the GOES disk area, resulting in a more precise observation of CF. The HT parameter does not represent the true physical height, but the radiatively equivalent height. The 5% coldest pixel in the IR histogram ($T_{5\%}$) is converted to HT in pressure units by interpolation of $T_{5\%}$ to a first guess temperature profile originating from a 6-h forecast.

3.2. *Evaluation methodology*

The radiation routines in forecast models compute solar and infrared radiation fluxes in broad bands (0.25–4 μm for solar radiation and 4–200 μm for infrared radiation). However, the GOES-7 satellite observes the radiation in relatively narrow frequency bands. Here, we have adapted the IR code of the model in order to compute the radiance (as opposed to flux) at the top of the atmosphere (TOA) in the specific 11 μm band of GOES-7 using spectroscopic parameters representative of that band. The radiative transfer equation for upward radiances yields the brightness temperature (TB):

$$\mathrm{TB}=P^{-1}\left[L_s^{\uparrow}t(p_s,0)+\int_{p_s}^{0}B(T_p)\frac{\partial t(0,p)}{\partial p}\,\mathrm{d}p\right],\qquad(11)$$

with

$$L_s^{\uparrow}=\varepsilon_s B(T_s)+(1-\varepsilon_s)L_s^{\downarrow}\qquad(12)$$

In (11), the term within brackets is the upward radiance; t is the product of the level-to-level upward transmissivities in the satellite direction of individual absorbers such as clouds and water vapor including the special absorption in the continuum region. T_s and p_s are the surface temperature (*skin*) and pressure; B is the Planck function and P^{-1} designates its inversion to equivalent temperature (The equivalent wave length used is 11.24 μm). $L_s^{\uparrow}$is the upward radiance at the surface and $L_s^{\downarrow}$ is the downward radiance at the surface computed by the radiative transfer equation for downward radiances, assuming a diffusivity factor of 1.66 (effective secant of zenith angle). The surface emissivity ε_s is set to unity over land while the ocean emissivity is parameterized as a function of satellite zenith angle following Schmetz (1986); it is over 0.992 for viewing angles less than 45°, decreasing to 0.972 at 60°. The water vapor transmissivity is computed in the same manner as in Garand (1983).

The calculation of TB was validated in clear sky condition over the ocean. The sky is considered clear if the CF parameter extracted from the satellite data is zero. Sea surface temperature and temperature and humidity profiles from the CMC operational analysis are used to calculate the TB that would be observed by satellite. The calculated TB was compared to that simultaneously observed by GOES-7 for the same location. The results based on over 9000 collocations show a mean error of 0.3 K in TB and a root mean square error (rmse) of 1.7 K. Then, calculations were done for all sky conditions using the model predicted temperature, humidity, and cloud water profiles along with the emissivity parameterizations described in Section 2. In this manner, TB from eq. (11) was verified with satellite observations.

In order to compare the simulated total cloud fraction (CF) with satellite observations, one has to combine the model simulated three dimensional cloud fraction (CF_l) into a total cloud fraction in each grid column in such a way that it corresponds to what the satellite observes. The model equivalent of CF is defined formally as one minus the cloud transmissivity through the entire atmosphere, using overlapping assumptions mentioned earlier, and assuming black clouds ($\varepsilon_l = 1$). Similarly a radiatively effective cloud fraction, ECF, which is the product of cloud fraction (output of the cloud condensation scheme) and the cloud emissivity, is then obtained if the emissivity parameterization is considered.

To get the model equivalent of HT, each grid mesh is divided into a number of atmospheric columns (sub-columns) with different radiative properties (clear, single-layered, and multiple layered column). To do this, the assumption of maximum-random overlapping of vertical cloud layers is used following a procedure described in Yu et al. (1996). For each sub-column, the atmospheric infrared window radiance that would be observed by GOES-7 is calculated. A histogram of infrared radiances is then constructed for each grid mesh with different IR radiances of these sub-columns. The 5% of the coldest radiance in the histogram is then converted to the equivalent cloud top temperature, and the corresponding pressure height (HT) is obtained by interpolation of the model temperature profile at the time of evaluation. A cloud top pressure of 1000 mb indicates a cloud free mesh, even over mountains where surface pressure may be lower than that value.

The above definitions of observed and modeled TB, CF and HT define the model evaluation methodology. 48-h forecasts at a resolution of about 100 × 100 km at the equator (119 waves, 21 vertical levels) were done starting daily from the 00 UTC analysis over a period of one month in order to reduce the influence of random errors in the initialization on the evaluation of the forecasts. The model outputs were interpolated to the grid of the satellite analysis which is 1 × 1 degree, very similar to that of the model. The model results were then compared with satellite observations for the same period. Because our objective is to evaluate the cloud condensation and cloud radiative property parameterization scheme, the forecast time at which the outputs are compared with the satellite data was chosen to be passed the model precipitation "spin-up" time (~6 h in midlatitudes, more in the tropics), yet short enough for the model accumulated errors not to become too large. In the present study, only the 24-h model clouds and IR radiation fields were evaluated with GOES data while sensitivity tests on global budgets were conducted for day 2 (24–48 h period) of the forecast.

4. Results

4.1. *Cloud fraction*

Table 2 shows the monthly averaged total cloud fraction derived from GOES-7 infrared and visible images versus the simulated one, based on 31 24-h forecasts valid at 00 UTC each day. The total

Table 2. *Monthly averaged total cloud fraction (%) observed from satellite data and derived from model output*

	GOES region	Over land	Over ocean
satellite data	54.9	58.3	53.6
model simulation	58.1	57.0	58.4

cloud fraction simulated by the model (58.1%) is a little larger than the observation (54.9%). Separation of land and oceanic regions reveals that largest differences occur over oceans (58.4% against 53.6%). Over land, the simulated total cloud fraction (57.0%) is comparable to the observed one (58.3%). Similar results were found in Dastoor (1994).

Fig. 1 shows the monthly accumulated histogram of the frequency of occurrence of clouds as a function of their spatial extent. Over the GOES region, the model tends to simulate more frequently cloud fractions around 50%, and less frequently overcast and clear sky cases (Fig. 1a). The land and ocean histograms show that the model simulates rather well the cloud occurrence over land (Fig. 1b), but significant differences occur over the tropical ocean region (Fig. 1c).

To understand the cloud amount differences, one needs to examine the geographical distribution of cloud fraction in order to evaluate if these model deficiencies are linked to certain climate regimes and/or atmospheric circulations. The geographical distribution of monthly mean CF is shown in Fig. 2. The model simulates relatively well the cloud fraction distribution in the middle and high latitude regions of both hemispheres compared with satellite data, especially over land. However, the cloud band in the ITCZ (Inter-Tropical Convergence Zone, here near 10°N) observed by satellite (Fig. 2a) is not well simulated (Fig. 2b). The underestimation of clouds in this region is in part due to underestimated low level (below 700 mb) humidity in the analyses to start the forecasts. This was verified using precipitable water observations from microwave imagery (Deblonde et al., 1996). The inaccuracy of the humidity fields in the tropics in the CMC analyses is mainly due to the lack of low level observations especially over oceans. Although the Humsat data used in 1993 improved the quality of humidity analyses at upper levels (Deblonde et al., 1995),

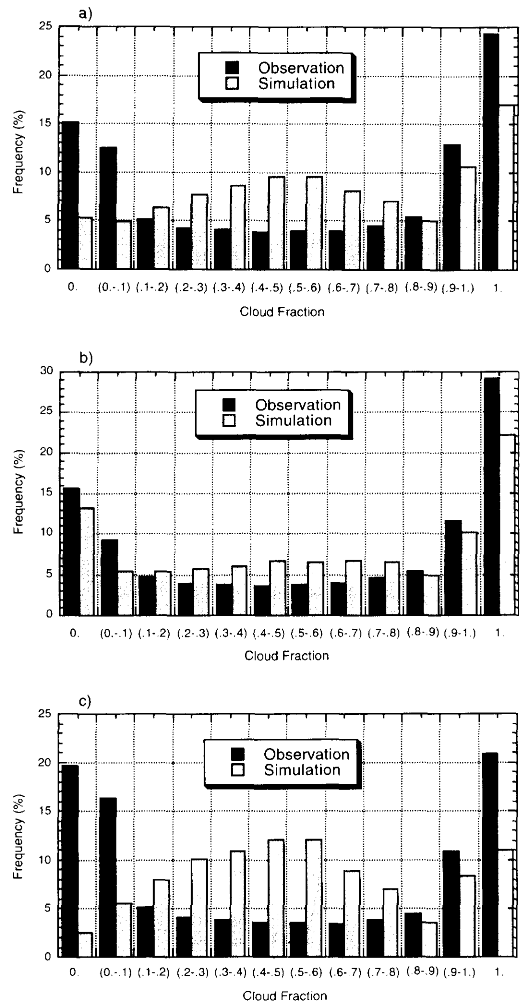

Fig. 1. Monthly accumulated histograms of cloud occurrence frequency as a function of their spatial extension. In horizontal axis, "0." represents clear sky, "1." overcast, "(0−0.1)" cloud fraction between 0. and 10%, etc. (a) entire GOES-7 domain statistics; (b) only over land; (c) over tropical ocean (30 S to 30 N).

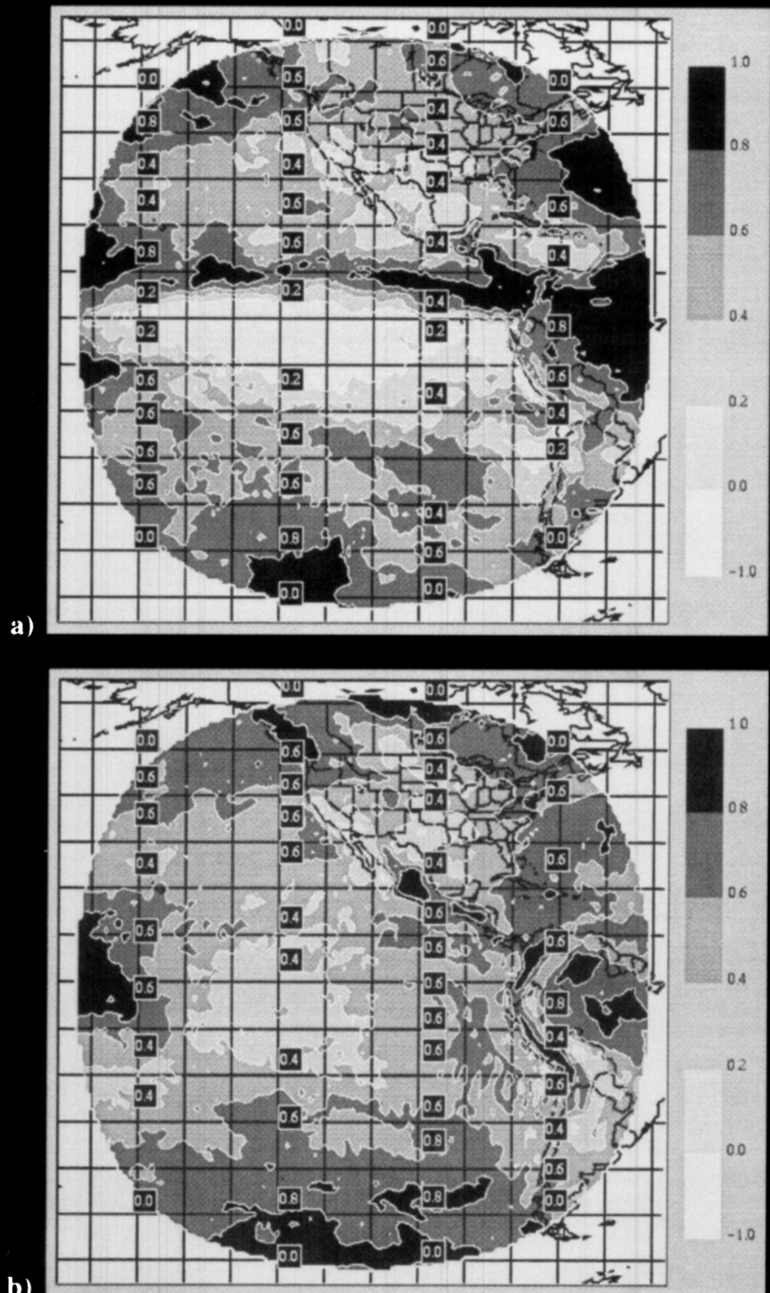

Fig. 2. Geographical distribution of the monthly averaged cloud fraction: (a) derived from GOES imagery; (b) derived from model output.

assigned too a low humidity in the clear areas of the ITCZ at low levels. As its name suggests, the ITCZ is a zone of moisture convergence at low levels; it can hold large amounts of precipitable water even in clear air (up to 45 mm). The Humsat scheme has been modified since then; the modifications include a more stringent quality control which ignores most clear air estimates at low levels.

Since we evaluate 24-h clouds/moisture forecasts in which the role of input moisture data has lowered with time, the noted ITCZ problem is likely dominated by deficiencies in the convection scheme. More recent forecasts (with Humsat problem corrected) based on October 1995 analyses and using a revised (more active) convective scheme indicate that the zonal mean day-2 precipitation rate at 10°N (peak of ITCZ) is 7.6 mm/day, slightly less than the October climatology found from microwave data: 8.7 mm/day (Deblonde et al., 1996); for comparison, our runs of October 1993 had a mean peak rain rate as low as 6.5 mm/day. The study of potential model deficiencies related to the convective cloud scheme or the strength of the ITCZ moisture convergence would require sensitivity studies outside the scope of this paper. It is also difficult, at present stage, to distinguish between the model errors in the tropics due to the quality of humidity analyses and those due to convection scheme, because the humidity fields in the CMC analyses, in the region where few observations are available, depend strongly on the first guess (6-h forecast) of the model.

In the subtropical anticyclonic region, the cloud fraction is largely over-estimated by the model (Fig. 2b) compared with the observed one, especially south of the ITCZ. In this region, the clouds are low ($\sim$900 mb) and moisture seems to be trapped in the boundary layer. This high humidity at low levels in the subtropics is potentially linked to the precipitation deficit in the ITCZ if moisture convergence is too weak from the subtropics to the ITCZ; the very same problem was noted in the ECMWF (European Center for Medium Range Forecasts) model by Soden and Bretherton (1994). On the west coasts of continents, especially over Mexico and South America mountains, a band of maximum cloudiness persists at high altitudes while a relatively cloud-free band on both sides of the mountains is simulated by the model. Although the satellite data give similar cloud characteristics over these regions, it seems that the topography effect is amplified or exaggerated in the model.

4.2. *Equivalent cloud top height*

Table 3 shows the monthly averaged cloud top height (in mb) derived from satellite data and retrieved from the model simulation (cloud-free cases are excluded in the averaging process). The satellite observation shows a mean cloud top of 559 mb in the GOES region, while the model simulates a mean cloud top of 633 mb, some 70 mb lower than that of observation. The cloud top is significantly higher over land (462 mb) than that over ocean (593 mb) in the satellite observations. Although the model gives, as for the observations, a higher cloud top over land (526 mb) than over the ocean (669 mb), the simulated cloud top is lower than that of observation by 60–70 mb both over land and ocean. Interpretation of these numbers requires examination of the maps of HT shown in Fig.3.

The distribution of the monthly averaged equivalent cloud top height from the simulation (Fig. 3b) is similar to that of the observation over land (Fig. 3a), especially over North America and the Brazilian forest. As seen for the cloud fraction (Fig. 2), the topographical effect is amplified in the model which results in a higher cloud top uphill and lower cloud top downhill. Largest differences take place over the ocean. The model underestimates the cloud top height west of Baja California, Chile and Peru although in these regions of oceanic stratocumulus, the model actually predicts larger cloud fraction than the observed one. The simulated cloud top is also not as high as that of the observation in the ITCZ region east of Hawaï, but the reverse is true west of Hawaï at the junction of the ITCZ with the SPCZ (South Pacific Convergence Zone, extending in the NW to SE direction).

Fig. 4a shows the monthly accumulated occurrence of cloud top as a function of pressure within the satellite disk area. Very high clouds (higher than 200 mb) and mid-level clouds (500–700 mb) are underestimated by the simulation, while the very low-level clouds (top lower than 900 mb) are largely overestimated. The underestimation of very high clouds and the overestimation of clouds between 200 mb and 300 mb are linked to the less

Table 3. *Monthly averaged cloud top pressure height (mb) observed from satellite data and derived from model output*

	GOES region	Over land	Over ocean
satellite data	559	462	593
model simulation	633	526	669

active deep convection in the tropics. The underestimation of mid-level clouds and the overestimation of very low-level clouds, especially over the ocean (Fig. 4b) are due to the incorrect water vapor in the boundary layer. In addition to refined humidity analyses, there seems to be a need for an improved shallow convection cloud scheme simulating more adequately the vertical water vapor transport in the model.

4.3. *Infrared radiance*

Fig. 5 shows the monthly averaged TOA IR radiance observed by GOES (Fig. 5a) and simulated by the model (Fig. 5b). There is a good agreement of the high/low IR radiance values between the observation and simulation. The subtropical oceanic regions are characterized by high IR radiance values due to relatively cloud-free conditions. The middle and high latitude regions are characterized by low IR radiance value due to large scale cloudiness and relatively low surface temperatures. The model simulates well the low IR radiance over the Brazilian forest associated with frequent occurrence of deep convection. Results are also satisfactory north of 30°N in general. However, the narrow band of low IR radiance associated with the ITCZ as revealed by satellite is not well simulated by the model, in line with previous discussion on CF and HT.

Fig. 6 shows zonal means of forecasted and observed CF, HT and TB; it summarizes best the evaluation results because the link between the three parameters is illustrated. South of 10°S (Fig. 6a), the zonal mean of simulated IR radiance is about 2 K warmer than the observed one. This is due to the lower cloud top height (Fig. 6b) and lower cloud water content (Deblonde et al., 1996) in the simulation although this effect is partly compensated by a larger cloud fraction (Fig. 6c) in these regions: the lower HT by about 100 mb with respect to observations are dominant over the higher cloud fraction by about 8%. The largest difference (about 8 K at 10°N) takes place in the ITCZ region because of the less active tropical convection in the simulation resulting in both too small cloud fraction (about 20% smaller than the observation) and too low cloud height (about 80 mb lower than the observation). The maximum difference on the cold side (Fig. 6a), 6 K, is noted at 3°S in the region of minimum observed cloud fraction of 30% as opposed to the simulated 50% cloud fraction (Fig. 6c).

The similitude between the observed and simulated TB in regions (e.g. between 25°N and 45°N) where cloud fraction and height are best predicted gives a positive indication that the chosen emissivity parameterization is quite reasonable. In contrast, the IR radiance calculated with the assumption of black clouds shows differences in TB reaching 20 K in the tropics (Fig. 6a).

5. Sensitivity of radiative budgets to assumed cloud optical properties

5.1. *Infrared optical properties*

In this section, we investigate further the cloud IR emissivity parameterization to visualize its impact on cloud transmittances, energy budgets and atmospheric cooling. Fig. 7 shows the global monthly averaged upward and downward cloud transmittances (t_c from the surface to each level and from the TOA to each level; these can be computed from the 3D cloud fraction, cloud water content, and temperature 24-h forecast fields) using the parameterizations described by eqs. (2), (5), and (6). The averaging process properly weights each grid column according to its horizontal area. For comparison, the transmittances are also computed with the assumption of black clouds. The upward transmittance with the parameterized cloud emissivity (solid line with circles) decreases rapidly with altitude near the surface,

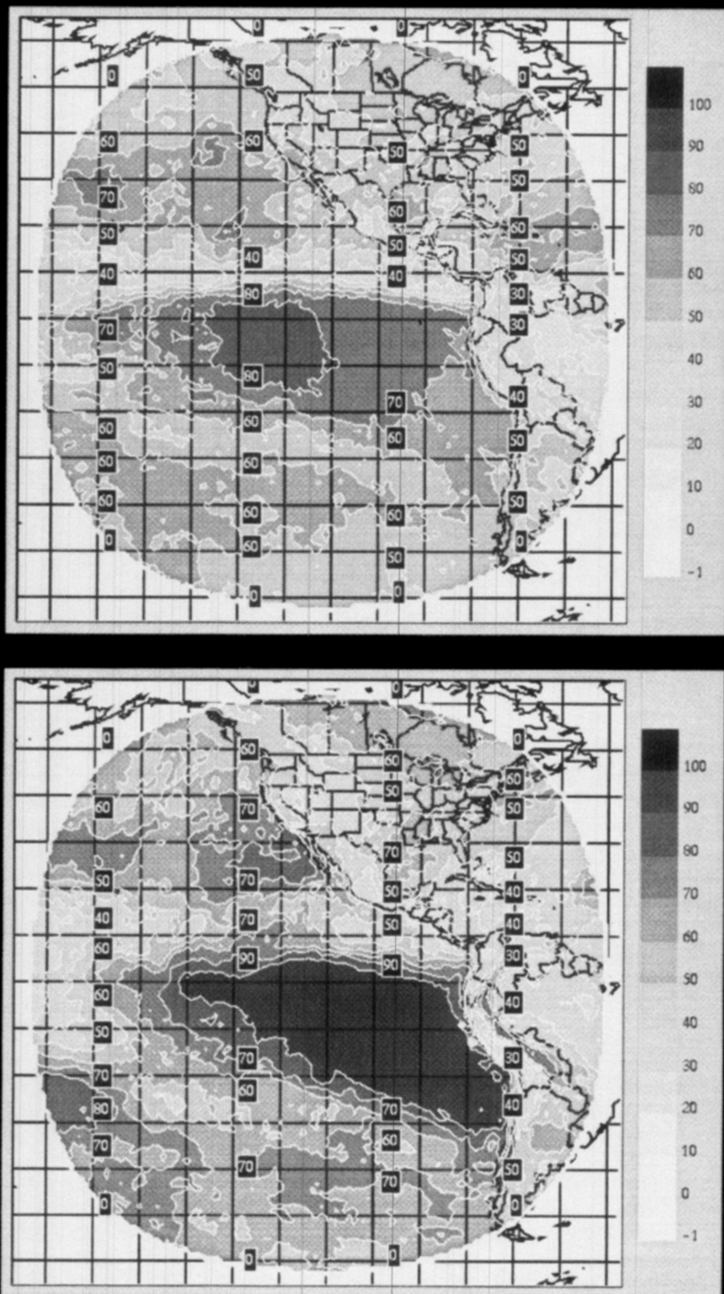

a)

b)

Fig. 3. Monthly averaged cloud top height expressed in pressure (mb): (a) derived from GOES imagery; (b) derived from model output.

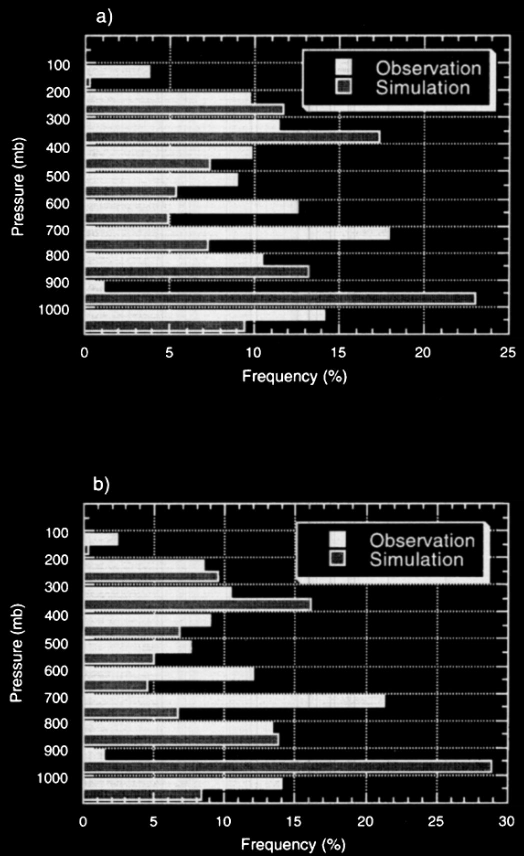

Fig. 4. Monthly accumulated histograms of cloud top occurrence frequency as a function of pressure in 100 mb intervals (1000 mb represents cloud-free situation): (a) over the entire GOES domain; (b) only over oceans.

from unity to 0.6 at $\sigma = p/p_s = 0.8$, due to the large low-level cloud fraction and water content in clouds, and then gradually to 0.52 at the top of the model atmosphere. The upward black-cloud transmittance (dashed line with squares) decreases more rapidly at low levels, in line with the maximum of cloud occurrence near 925 mb shown in Fig. 4. Further upwards, the two curves decrease at about the same rate up to $\sigma = 0.4$. At higher levels, there is another rapid decrease of transmittance between $\sigma = 0.4$ and $\sigma = 0.2$, which does not appear in the grey-cloud curve. This difference is due to the treatment of cloud radiative properties for semi-transparent ice clouds in relation with the maximum in cloud frequency occurrence noted at 350 mb in Fig. 4. Similarly, the rapid decrease of downward transmittance (dashed line with crosses) above $\sigma = 0.4$ for black clouds is not observed in the curve with parameterized cloud emissivity (solid line with triangles). These curves represent another way (not yet explored, we believe) to examine the radiative impact of clouds *as a function of height* rather than just their effect on TOA or surface fluxes. If the climatology of the transmittance with black clouds as a function of height was known, it could be used for evaluating the 3-D cloud structure and cloud overlapping assumption in the model as well. From there, if the climatology of the grey-cloud curve was known it could be used for evaluating the cloud optical property parameterization.

To evaluate the global average impact of the parameterization on the IR cooling rates, two 48-h forecasts were done: one with the assumption of black clouds, the other with the parameterized cloud emissivity. Table 4 summarizes the longwave radiation budget for day 2 of a forecast based on the 28 October 1993 00 UTC analysis. The net outgoing longwave radiation at the top of the atmosphere increases from 208.8 W/m^2 in the black-cloud experiment to 242.7 W/m^2 in the grey-cloud experiment. The atmospheric radiation differs by 26 W/m^2 (corresponding to 1.54 K/day mean atmospheric cooling for grey clouds, but only 1.30 K/day for black clouds); the surface net radiation differs by 8 W/m^2. While the sign of the differences was expected from previous arguments, the magnitude of the differences is worth noting. For comparison, the global mean October budget from Rossow and Zhang (1995) is shown; it is derived from ISCCP observed clouds coupled with a radiative transfer model. A fair comparison would imply to evaluate the model monthly climatology, but experience shows that the day of the month has only a modest impact (a few W/m^2, see Rossow and Zhang, 1995) on globally averaged budgets. It is seen that the atmospheric budget (hence mean cooling rate) of the forecast with emissivity parameterization is very close to the climatology, while flux differences at the top and surface of about 10 W/m^2 are obtained. The TOA differences can be explained by Fig. 6a where warmer TOA brightness temperatures in the ITCZ and in the southern hemisphere were noted. Insisting to get exactly the same budget as that of the ISCCP or ERBE observations of outgoing radiation will only compensate for errors in the

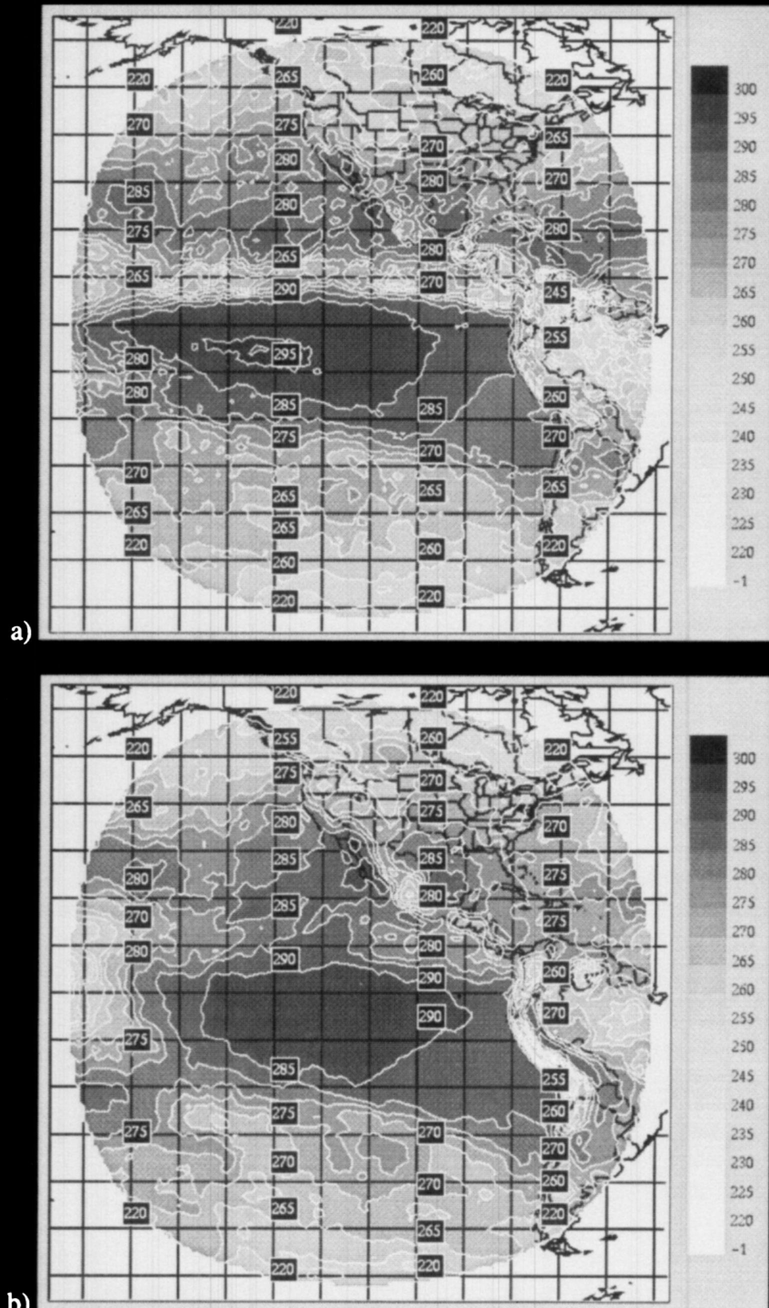

Fig. 5. Monthly averaged infrared radiance (10–12 μm) expressed in equivalent brightness temperature (K): (a) satellite observation; (b) model simulation.

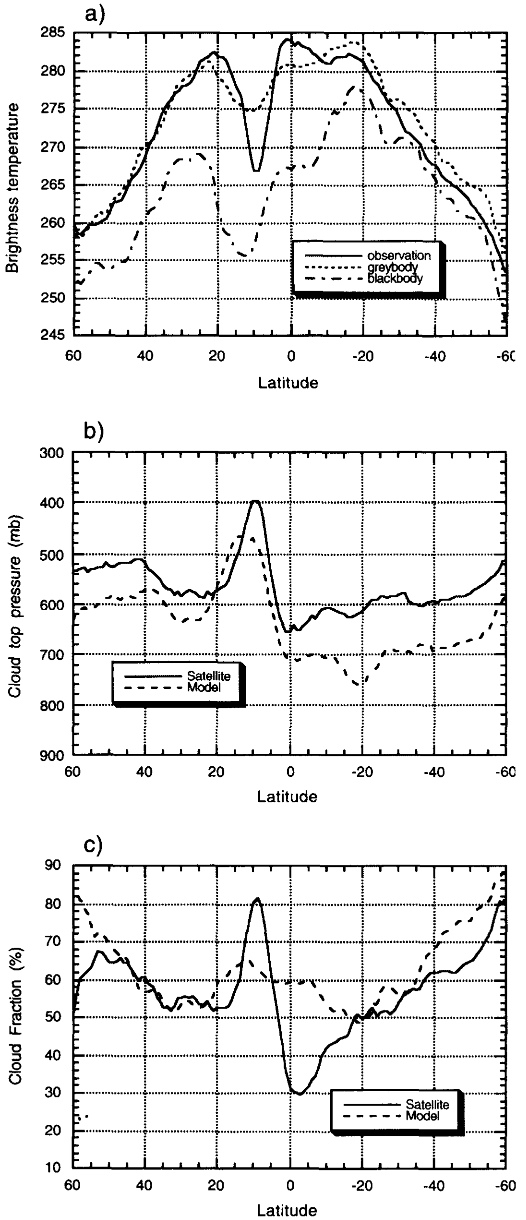

Fig. 6. (a) Zonal mean of the monthly averaged infrared radiance (10–12 μm) expressed in equivalent brightness temperature (K), obtained from satellite observation (solid), calculated from model output using a parameterized cloud emissivity (dotted) and using a cloud emissivity of unity (dash-dot). (b) Zonal mean of the monthly averaged cloud top pressure height (mb) derived from satellite observation (solid) and model output (dashed) respectively. (c) Zonal mean of the monthly averaged cloud fraction derived from satellite observation (solid) and model output (dashed).

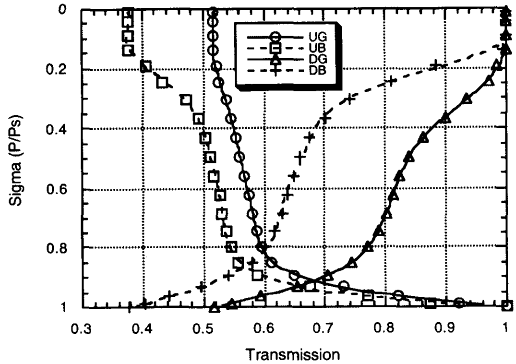

Fig. 7. Monthly averaged atmospheric upward and downward transmittance calculated from the model simulated cloud fraction and cloud water content. UG/DG: upward/downward transmittances with the assumption of grey clouds (parameterized emissivity); UB/DB: upward/downward transmittances with the assumption of black clouds.

cloud distributions and therefore make the regional budgets worse than the compromise reached in Fig. 6a. Also, uncertainties remain in the surface budget as it is derived from calculations subject to errors in cloud base, assumed cloud radiative properties, and overlapping assumptions (Charlock et al., 1994). As another comparison, the ECMWF model IR budget presented by Morcrette (1990) was 244 W/m^2 at the TOA and 67 W/m^2 at the surface.

Fig. 8 shows the latitudinal distributions of effective cloud fraction (ECF) respectively for black-cloud and grey-cloud assumptions, and the global mean values. The global mean ECF decreases from 67% in the black-cloud assumption to 51% in grey-cloud assumption. Largest differences, as expected, are found at high latitudes where the nominal cloud fraction is in the 90–100% range whereas the effective cloud fraction is in the 30–70% range. Differences of about 20% are also noted in the ITCZ where cirrus are formed in the convective environment. In the midlatitudes, typical differences are 4–7% between the nominal and effective cloud fraction. The global nominal cloudiness of 67% is slightly larger than the ISCCP estimate of 63% (Rossow et al., 1993). The model CF estimates in polar regions

Table 4. *Global averaged longwave radiation (losses in W/m²) for day 2 of a forecast assuming black/grey clouds; October means from the ISCCP study of Rosscow and Zhang (1995) are also shown*

	Black clouds	Grey clouds	ISCCP
net radiation at the top	208.8	242.7	233.8
atmospheric radiation	161.5	187.3	189.4
net surface radiation	47.3	55.3	44.4

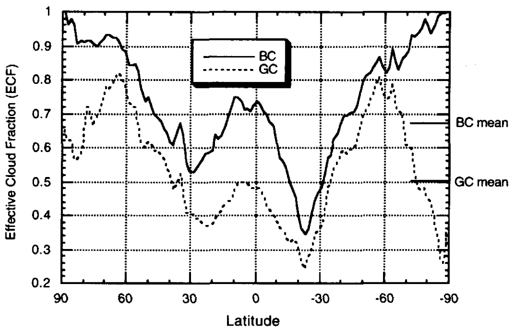

Fig. 8. Zonal mean of effective cloud fraction (ECF) for grey (GC) and black (BC) clouds; global average indicated on the right.

are likely overestimated, but Fig. 8 clearly indicates that the total cloud amount there is highly influenced by very thin ice clouds which may not be detectable by satellite or even by observers. If black clouds imply a global surface relative warming equivalent to 8 W/m² (Table 4), over polar regions zonal plots (not shown) indicate a larger warming effect corresponding to about 40 W/m², with 50 W/m² over the South Pole and 30 W/m² over the North pole (latitudes 80°-90°). This result is close to the 40 W/m² surface warming effect of black clouds quoted by Curry and Ebert (1992) from their one-dimensional model simulations.

5.2. *Shortwave optical properties*

As noted in the introduction, our evaluation with GOES-7 imagery was limited to clouds and infrared radiation. It is nevertheless possible to evaluate if the solar budget resulting from the new cloud parameterization matches the expected climatology. We find that the parameterizations of shortwave cloud optical properties described in Section 2 give on a global basis a planetary albedo which is too high, 39%, coupled with a surface downward flux of 150 W/m², a value which is too low by about 10 W/m². It is well established from satellite observations that the planetary albedo is near 30%. However, the partition of the energy between what reaches the surface and what is absorbed by the atmosphere is still a subject of debate with numbers varying between 150 W/m² and 185 W/m² for the surface net flux. The recent investigation of Li and Leighton (1993) suggests a value of 160 W/m² and a planetary albedo of 29.7%. As seen in Table 5, the Rossow and Zhang study (1995, based on ISCCP) yields a similar downward flux (165 W/m²), but a higher planetary albedo of 32.4% and a significantly less absorbing atmosphere (by 21 W/m² translating into a 0.2 K/day difference in mean atmospheric heating rate). The higher atmospheric heating is likely due to a lower single scattering albedo, the parameter controlling the droplet absorption. The absorption is small for wavelengths below 1 μm, but increases in the near infrared (1–4 μm). Clearly, splitting the spectrum into four or more sub-intervals would be desirable if operational constraints can allow it.

The October budget in the ISCCP study is identical to within 1 W/m² to the annual mean budget. We tried to align our budgets to those of the ERBE study because the outgoing radiation is directly observed. As shown in Table 5, that result can be obtained if the optical depth is reduced to 28% of the value proposed by the parameterization, keeping the other parameters unchanged. This is shown using as a typical example the same 28 October forecast as in the previous section. The concept of a reduced effective optical thickness has been discussed by Harshvardan and Randall (1985), and more recently by Cahalan et al (1994), who quoted reduction factors for global budgets similar to the one found in this study. It is necessary to reduce the optical thickness to take into account inhomogeneities in the distribution of cloud water in a

Table 5. *Global solar budget for the 24-h forecast issued 28 October 1993 in comparison with ERBE (Li and Leighton, 1993) and ISCCP (Rossow and Zhang, 1995) annual estimates. Fluxes in W/m²; % of incoming energy in parentheses*

	Forecast	ERBE	ISCCP
incoming at the TOA	346	341	342
outgoing at the TOA	105 (30.3)	101 (29.7)	111 (32.5)
atmospheric absorption	84 (24.3)	83 (24.3)	65 (19.1)
net at the surface	157 (45.4)	157 (46.0)	165 (48.3)

model grid box and to compensate for the assumption of a plane-parallel atmosphere as revealed by Cahalan et al. (1995), and that of random overlap of cloud layers implicit in the solar radiation code. Both the global solar and infrared radiation budget and the comparison of LWP with that retrieved from microwave imagery (Deblonde et al., 1996) imply that the global mean LWP is in the reasonable range although regional differences exist. It is expected that improvements on the representation of clouds in solar radiation (plane-parallel and random overlap assumptions) and on the simulation of regional distribution of LWP would help a lot to reduce the uncertainties in the solar radiation budget.

Although reasonable global shortwave budgets are obtained, much remains to be done to ensure proper local calculations of solar fluxes taking into account factors such as cloud morphology and cloud water inhomogeneities. The sensitivity to r_e, f_w and N was evaluated. Changing the ice effective radius from 25 μm to 15 μm reduces the net shortwave surface flux by 2.1 W/m² and increases the TOA reflected flux by 3.3 W/m² (TOA albedo by 0.9%). The influence on the IR budget is also non negligible: the TOA and atmospheric fluxes decrease by 5.7 W/m² and 4.7 W/m² respectively while the net surface flux lowers by 1 W/m². Thus the budgets using an effective ice radius of 15 μ appear slightly improved, notably at the TOA. The effect of N and r_e on the radiative budgets was evaluated by Boucher et al. (1995). Using values suggested by these authors of $N=50$ over ocean and $N=200$ over land in eq. (10) resulted in decreasing the TOA flux by 1.6 W/m² and increasing the net surface flux by 3.6 W/m². The water phase probability f_w varies with cloud type (Matveev, 1984) and complex physical factors. Using various functions published in the literature did not affect significantly the IR budget and only marginally the shortwave budget (less than 1 W/m²). However, in the extreme case where all clouds are assumed in ice phase below 0°C, the shortwave net surface flux increases by 10 W/m² and the TOA reflected flux decreases by 3 W/m².

6. Concluding remarks

The model simulated cloud properties (cloud fraction, top height) and IR radiance are compared to those from GOES-7 satellite observations over a monthly period using a model-to-satellite approach where model output is transformed into quantities routinely analyzed with satellite data. A model that carries cloud water as a prognostic variable was evaluated in view of an eventual implementation at the CMC. Such a model represents a significant progress towards more realistic modeling of moist processes and cloud/radiation interactions.

It is found that the model simulates well the cloud fraction in the middle and high latitude regions of both hemispheres. The geographical distributions of the model simulated cloud top height and IR radiance are similar to those from satellite data, although the model simulates lower cloud tops and warmer IR radiance especially in the tropics when compared with those observed by satellite. In particular, there is an underestimation of cloud cover and cloud top height in the ITCZ in the model simulation. The other most obvious problem is that too much boundary clouds with lower top height are noted in the subtropics when compared to those from satellite observations. These deficiencies are at least partially linked to imperfect initial humidity fields. The assimilation of SSM/I integrated water vapor observations in the analysis should prove very useful over oceans. Work is under way to improve the convection scheme and boundary layer humidity transport.

The large impact of the emissivity parameterization is examined by comparison of the IR budget, transmittances and cooling rates with those obtained in the extreme case where all clouds are assumed black. We find that the chosen IR emissivity parameterization yields realistic budgets without any additional adjustment. The global shortwave budget also matches well available climatology after adjustment of the optical thickness. The fact that radiation characteristics are quite good in regions where clouds are realistic gives good confidence that the modeled cloud radiative properties are correct to first order. Improving the representation of clouds remains the main requirement to get good radiation budgets at all latitudes. In that regard we find that the clouds of the prognostic cloud water scheme used in this study are clearly superior to those of the current operational model. Work is still required in the shortwave domain to take into account cloud water inhomogeneity effects and spectral dependencies of cloud optical properties. The evaluation methodology could be applied routinely and extended to other infrared bands and to visible wavelengths.

7. Acknowledgments

Discussions with C. Girard, G. Deblonde and H. Barker contributed to the improvement of this manuscript. B. Bilodeau, C. Beaudouin, and B. Dugas are thanked for their technical support. We thank the anonymous reviewers for their valuable comments and suggestions which improve the technical presentation of this manuscript. The research was supported by the Natural Sciences and Engineering Research Council of Canada through a visiting fellowship for Canadian Government Laboratories.

REFERENCES

Barker, H. W. 1992. Solar radiative transfer through clouds possessing isotropic variable extinction coefficient. *Quart. J. Roy. Meteor. Soc.* **118**, 1145–1162.

Bony, S., Le Treut H., Duvel, J. P. and Kandel, R. S. 1992. Satellite validation of GCM-simulated annual cycle of the Earth radiation budget and cloud forcing. *J. Geophys. Res.* **97** (D16), 18061–18081.

Boucher, O., Le Treut, H. and Baker, M. B. 1995. Precipitation and radiation modeling in a general circulation model: introduction of cloud microphysical processes. *J. Geophys. Res.* **100** (D8), 16395–16414.

Cahalan, R. F., Ridgway, W., Wiscombe, W. J., Bell, T. L. and Snider, J. B. 1994. The albedo of fractal stratocumulus clouds. *J. Atmos. Sci.* **51**, 2434–2455.

Cahalan, R. F., Silberstein, D. and Snider, J. B. 1995. Liquid water path and plane-parallel albedo bias during ASTEX. *J. Atmos.Sci.* **52**, 3002–3012.

Charlock, T. P., Rose, F., Alberta, T., Smith, G. L., Rutan, D., Manalo-Smith, N., Minnis, P. and Wielicki, B. 1994. *Cloud profiling radar requirements: perspective from retrievals of the surface and atmospheric radiation budget and studies of atmospheric energetics. Utility and feasability of a cloud profiling radar.* Report of the GEWEX Topical Workshop (Pasadena, California, USA, 29 June–1 July 1993) WMO/TD-No 593, pages B10–B21.

Curry, J. A., and Ebert, E. E. 1992. Annual cycle of radiation fluxes over the Arctic ocean, Sensitivity to cloud optical properties. *J. Climate* **5**, 1267–1280.

Dastoor, A. P. 1994. Cloudiness parameterization and verification in a large-scale atmospheric model. *Tellus* **46A**, 615–634.

Deblonde, G., Garand, L., Gauthier, P. and Grassotti, C. 1995. Assimilation of SSM/I and GOES humidity retrievals with a one-dimensional variational analysis scheme. *J. Appl. Meteor.* **34**, 1536–1550.

Deblonde, G., Yu, W., Dastoor, A. and Garand, L. 1996. Validation of global NWP analyses and forecasts using DMSP SSM/I retrievals. Part II: Model/Analyses inter comparison with SSM/I retrievals, *J. Geophys. Res.* in press.

Ebert, E. E. and Curry, J. A. 1992. A parameterization for ice optical properties for climate models. *J. Geophys. Res.* **97** (D4), 3831–3836.

Fouquart, Y. and Bonnel, B. 1980. Computations of solar heating of the earth's atmosphere. A new parameterization. *Contr. Atmos. Phys.* **53**, 35–62.

Garand, L. 1983. Some improvements and complements to the infrared emissivity algorithm including a parameterization of the absorption in the continuum region. *J. Atmos. Sci,* **40**, 230–244.

Garand, L. 1993. A pattern recognition technique for retrieving humidity profiles from Meteosat or GOES imagery. *J. Appl. Meteor.* **32**, 1592–1607.

Garand, L. and Mailhot, J. 1990. The influence of infrared radiation on numerical weather forecasts. *Proceedings of the 7th Conference on Atmospheric radiation*, 23–27 July 1990, San Francisco. *Amer. Meteor. Soc.*, J146–151.

Geleyn, J-F. and Hollingsworth, A. 1979. An economical analytical method for the computation of the interaction between scattering and line absorption of radiation. *Contrib. Atmos. Phys.* **52**, 1–16.

Harshvardan and Randall, D. A. 1985. Comments on "The parameterization of radiation for numerical weather prediction and climate models". *Mon. Wea. Rev.* **113**, 1832–1833.

Li, Z., and Leighton, H. G. 1993. Global climatology of solar radiation budgets at the surface and in the atmosphere from 5 years of ERBE data. *J. Geophys. Res.* **98**, (D3), 4919–4930.

Matveev, L. T. 1984. *Cloud dynamics* Atmospheric Science Library, D. Reidel Publishing Company, 340 pp.

Morcrette, J. J. 1990. Impact of changes to the radiation transfer parameterizations plus cloud optical properties in the ECMWF model. *Mon. Wea. Rev.* **118**, 847–873.

Morcrette, J. J. 1991. Evaluation of model-generated cloudiness: satellite-observed and model-generated diurnal variability of brightness temperature. *Mon. Wea. Rev.* **119**, 1205–1224.

Ritchie, H. 1991. Application of the semi-Lagrangian method to a multilevel spectral primitive-equation model. *Quart. J. Roy. Meteor. Soc.* **117**, 91–106.

Rockel, B., Raschke, E. and Weyres, B. 1991. A parameterization of broad band radiative transfer properties of water, ice, and mixed clouds. *Beitr. Phys. Atmosph.* **64**, 1–12.

Rossow, W. B., Walker, A. W. and Garder, L. C. 1993. Comparison of ISCCP and other cloud amounts. *J. Climate* **6**, 2394–2418.

Rossow, W. B. and Zhang, Y.-C. 1995. Calculation of flux of the atmosphere radiative fluxes from physical quantities based on ISCCP datasets 2. Validation and first results. *J. Geophys. Res.* **100** (D1), 1166–1197.

Schmetz, J. 1986. An atmospheric-correction scheme for operational application to Meteosat infrared measurements. *ESA Journal.* **10**, 145–159.

Slingo, A. 1989. A GCM Parameterization for the shortwave radiative properties of water clouds. *J. Atmos. Sci.* **46**, 1419–1427.

Soden, B. J. and Bretherton, F. P. 1994, Evaluation of water vapor distribution in general circulation models using satellite observations. *J. Geophys. Res.* **99** (D1), 1187–1210.

Stephens, G. L. 1978. Radiative properties of extended water clouds. 2. *J. Atmos. Sci.* **35**, 2123–2132.

Sundqvist, H., Berge, E. and Kristjansson, J. E. 1989. Condensation and cloud parameterization studies with a mesoscale Numerical Weather Prediction model. *Mon. Wea. Rev.* **117**, 1641–1657.

Yu, W., Sèze, G., Le Treut, H. and Desbois, M. 1991. Comparison of radiance fields observed by satellite and simulated by the LMD general circulation model. *Dynam. of Atmos. and Oceans.* **16**, 147–165.

Yu, W., Doutriaux, M., Sèze, G., Le Treut, H. and Desbois, M. 1996. A methodology study of the validation of clouds in GCMs using ISCCP satellite observations. *Climate Dynamics* **12**, 389–401.